Case Report | Gastrointestinal Imaging

http://dx.doi.org/10.3348/kjr.2013.14.5.769
pISSN 1229-6929 · eISSN 2005-8330
Korean J Radiol 2013;14(5):769-775

Korean Journal of Radiology
KJR

Diffusion-Weighted MRI in Intrahepatic Bile Duct Adenoma Arising from the Cirrhotic Liver

Chansik An, MD[1], Sumi Park, MD[2], Yoon Jung Choi, MD[3]

[1]Department of Radiology, Research Institute of Radiological Science, Severance Hospital, Yonsei University College of Medicine, Seoul 120-752, Korea; Departments of [2]Radiology and [3]Pathology, National Health Insurance Corporation Ilsan Hospital, Goyang 410-719, Korea

A 64-year-old male patient with liver cirrhosis underwent a CT study for hepatocellular carcinoma surveillance, which demonstrated a 1.4-cm hypervascular subcapsular tumor in the liver. On gadoxetic acid-enhanced MRI, the tumor showed brisk arterial enhancement and persistent hyperenhancement in the portal phase, but hypointensity in the hepatobiliary phase. On diffusion-weighted MRI, the tumor showed an apparent diffusion coefficient twofold greater than that of the background liver parenchyma, which suggested that the lesion was benign. The histologic diagnosis was intrahepatic bile duct adenoma with alcoholic liver cirrhosis.

Index terms: *Bile duct adenoma; Peribiliary gland hamartoma; Diffusion-weighted imaging; Apparent diffusion coefficient; Gadoxetic acid-enhanced MRI*

INTRODUCTION

Intrahepatic bile duct adenoma (BDA) is a rare benign tumor of the liver arising from the epithelium of the intrahepatic bile ducts. Research has suggested that this benign tumor should be called a peribiliary gland hamartoma because of a similarity between bile duct adenoma and peribiliary glands in their secretory gland-cell phenotype (1). According to Edmondson's classification (2), bile duct adenoma is the rarest of benign primary hepatic tumors, with an incidence of 1.3%. Craig et al. (3) reported that bile duct adenoma was identified in only five of 50000 autopsies. Often, bile duct adenoma is depicted as a well-defined, non-encapsulated, non-cystic small (< 2 cm) tumor typically found on the surface of the liver. Due to its characteristic subcapsular location and small size, most cases have been found incidentally on autopsies or resected livers after treatment for other pathologies (2-4). Histologically, bile duct adenoma is characterized by inflammation and fibrosis involving a proliferation of bile ductules, which are thought to be reactive processes in response to focal injuries and may be associated with chronic liver disease (4).

We report imaging features of a case of surgically confirmed intrahepatic BDA. To our knowledge, this is the first report of a case of intrahepatic BDA that was studied using both diffusion-weighted imaging (DWI) and gadolinium-ethoxybenzyl-diethylene triamine pentaacetic acid (Gd-EOB-DTPA)-enhanced magnetic resonance imaging (MRI).

CASE REPORT

A 64-year-old male patient with alcoholic liver cirrhosis, who was under surveillance for hepatocellular carcinoma

Received April 18, 2013; accepted after revision May 12, 2013.
Corresponding author: Sumi Park, MD, Department of Radiology, National Health Insurance Corporation Ilsan Hospital, 100 Ilsan-ro, Ilsandong-gu, Goyang 410-719, Korea.
• Tel: (8231) 900-0837 • Fax: (8231) 900-0056
• E-mail: smp0304@nhimc.or.kr

(HCC), showed a mass-like lesion on a computed tomography (CT) scan. The CT scan performed 22 months earlier had revealed no abnormal lesion in the liver. Liver function tests on admission showed elevated serum aminotransferases, with a glutamic-oxaloacetic transaminase level of 121 IU/L (normal = 15-41 IU/L) and a glutamic-pyruvic transaminase level of 69 IU/L (normal = 17-59 IU/L). The serological workups for the hepatitis B virus antigen and hepatitis C virus antibody were negative, and the serum alpha-fetoprotein level was normal.

Dynamic CT scan was performed with a multi-detector row scanner (Somatom Definition Flash, Siemens Healthcare, Forchheim, Germany) before and after the intravenous injection of 2 mL/kg of non-ionic, iodinated contrast material (Xenetix 300, iobitridol; Guerbet, Sulzbach, Germany). Unenhanced images showed a newly developed 1.4-cm low-density subcapsular mass in the left lateral segment of the liver (Fig. 1A). On dynamic contrast-enhanced images, the mass demonstrated homogeneous enhancement in the arterial phase (18 seconds after the injection of contrast material) and persistent enhancement in the portal venous phase (60 seconds) but appeared to be isoattenuated relative to the liver parenchyma in the delayed phase (180 seconds) (Fig. 1B-D). The CT parameters were as follows: detector collimation, 0.63 mm; reconstruction interval, 3 mm; tube voltage, 120 kVp; and

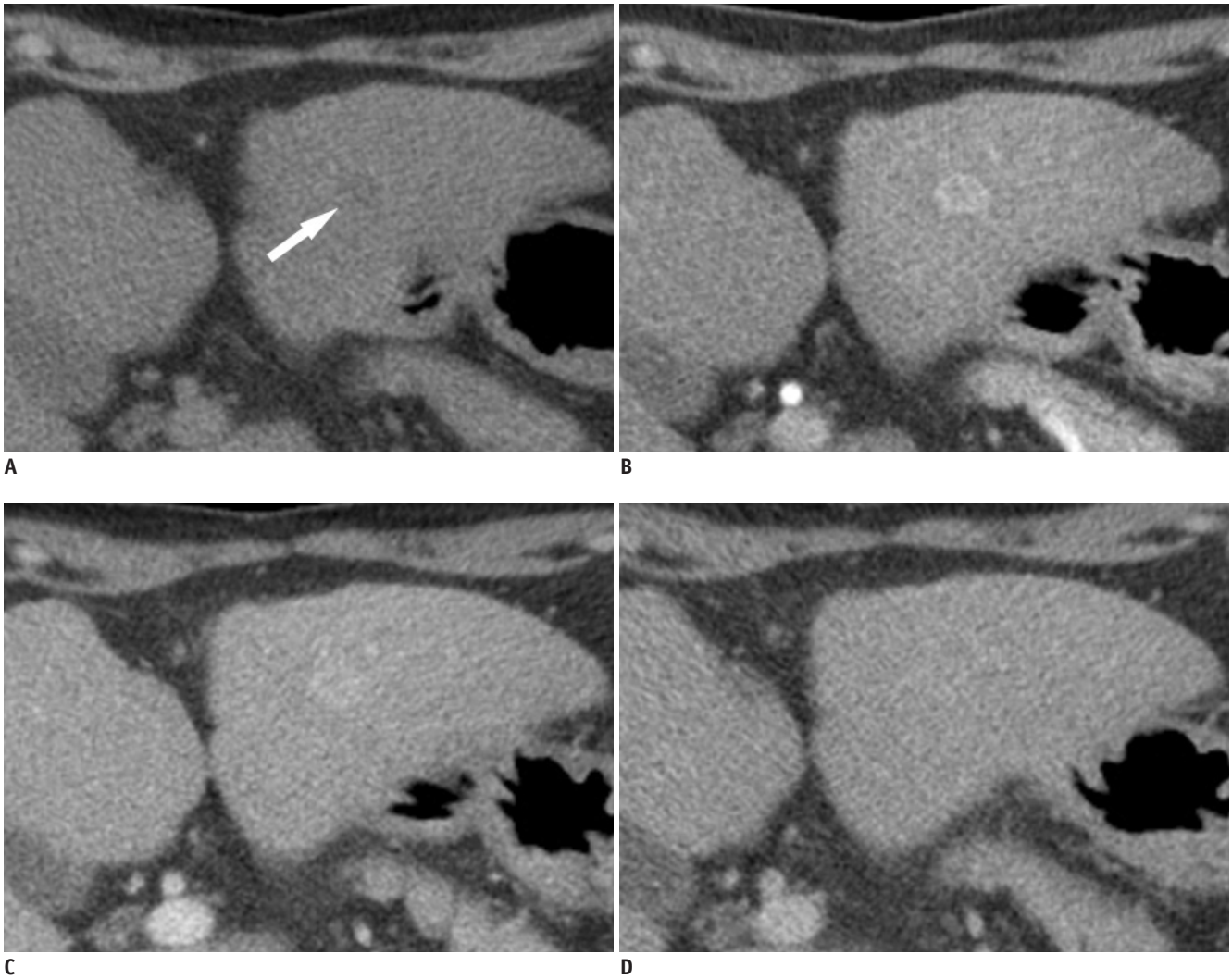

Fig. 1. Dynamic contrast-enhanced CT images, Gd-EOB-DTPA-enhanced and diffusion-weighted MR images, and pathologic findings in 64-year-old male with intrahepatic bile duct adenoma.
Dynamic contrast-enhanced CT images. **A.** Unenhanced CT scan shows well-defined low density nodule measuring about 1.4 cm in lateral segment of left hepatic lobe (arrow). Note nodular surface and blunted margin of liver, indicative of liver cirrhosis. **B.** Dynamic contrast-enhanced CT scan reveals arterial enhancement of nodule. **C.** In portal venous phase, nodule shows persistent enhancement. **D.** In delayed phase, tumor is not well delineated because of its isodensity to adjacent liver parenchyma. Gd-EOB-DTPA = gadolinium-ethoxybenzyl-diethylene triamine pentaacetic acid

Korean Journal of Radiology
KJR

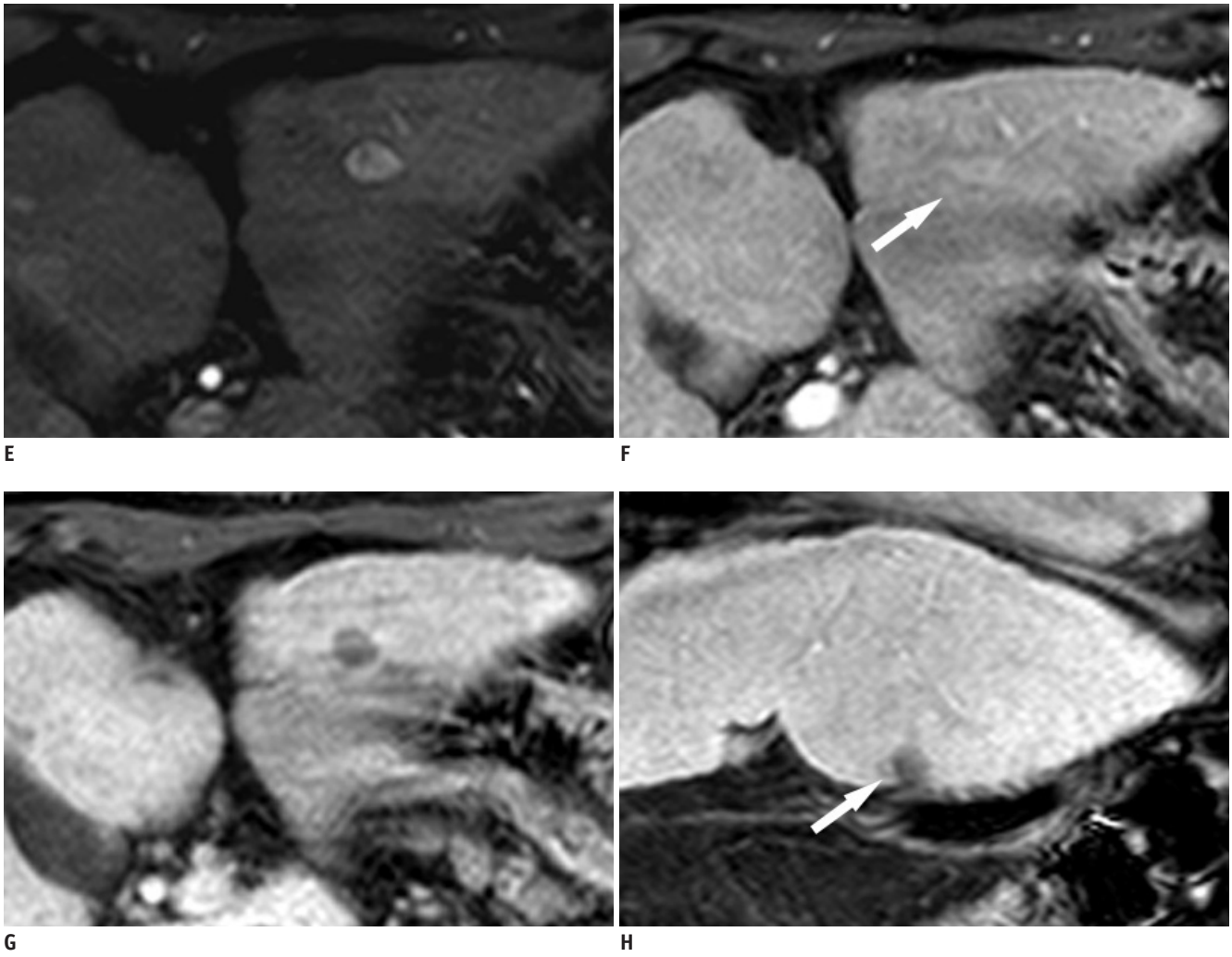

Fig. 1. Dynamic contrast-enhanced CT images, Gd-EOB-DTPA-enhanced and diffusion-weighted MR images, and pathologic findings in 64-year-old male with intrahepatic bile duct adenoma.
Dynamic Gd-EOB-DTPA-enhanced and diffusion-weighted MR images. **E, F.** Tumor shows strong enhancement in arterial phase **(E)**, persistent enhancement in portal venous phase, but isointensity in late dynamic phase (**F**, arrow). **G, H.** Transverse **(G)** and coronal **(H)** hepatobiliary phase images demonstrate that nodule, in its subcapsular location (arrow) shows distinctly low signal intensity. Gd-EOB-DTPA = gadolinium-ethoxybenzyl-diethylene triamine pentaacetic acid

the product of the tube current and exposure time, 50-240 mAs in conjunction with dose modulation techniques.

Liver dynamic MRI was performed one week later to rule out the possibility of small HCC with a 3-T whole-body MRI system (Intera Achieva 3.0T, Philips Medical System, Best, the Netherlands). On T2-weighted images, the mass showed high signal intensity. On T1-weighted images, it showed low signal intensity. On dynamic MRI using Gd-EOB-DTPA (Primovist, Bayer Schering Pharma, Berlin-Wedding, Germany; 0.025 mmol/kg), the mass showed strong enhancement in the arterial and portal venous phases (30 and 70 seconds after the injection of Gd-EOB-DTPA, respectively) but was isointense to the liver parenchyma in the late dynamic phase (180 seconds) (Fig. 1E, F). In hepatobiliary phase images, which were obtained 20 minutes after the injection, the mass was distinctly hypointense (Fig. 1G, H). Respiratory-triggered DWI sequences were performed with single-shot echo planar imaging with b values of 0, 50, 400, and 800 s/mm^2. The apparent diffusion coefficient (ADC) was automatically calculated by the MR system and displayed as the corresponding ADC map. The mass showed high signal intensity on DWI even at high b-values and exhibited high signal intensity on the ADC map. The ADC value (2.21×10^{-3} mm^2/s) of the tumor was more than twofold that of the surrounding liver parenchyma (1.01×10^{-3} mm^2/s), which indicates that the hyperintensity seen on high b-value DWI was due to a very high signal intensity on T2-weighted

images rather than diffusion restriction (Fig. 1I, J).

Initially, our first impression was that the patient had a benign enhancing nodule, such as focal nodular hyperplasia (FNH), FNH-like lesion, small hemangioma or dysplastic nodule. However, the possibility of HCC could not be ruled out. When all the possible diagnoses were explained to the patient, he chose to have the mass resected and underwent left lateral segmentectomy at our institution.

A gross inspection of the specimen showed an ill-defined yellowish nodule located about 0.5 cm from the hepatic capsule, measuring about 1.2 x 1 cm. Microscopically, a proliferation of well-formed bile ductules on a background of fibrous stroma was noted without cellular atypia or mitotic activity (Fig. 1K, L). The result from immunohistochemical stain was negative for carcino-embryonic antigen and p53, but positive for cytokeratin-19. The absence of p53 helps differentiate bile duct adenoma from metastatic adenocarcinoma. The presence of cytokeratin-19 shows that the nodule is of bile duct origin (5). The histologic diagnosis was intrahepatic bile duct adenoma on a background of alcoholic liver cirrhosis.

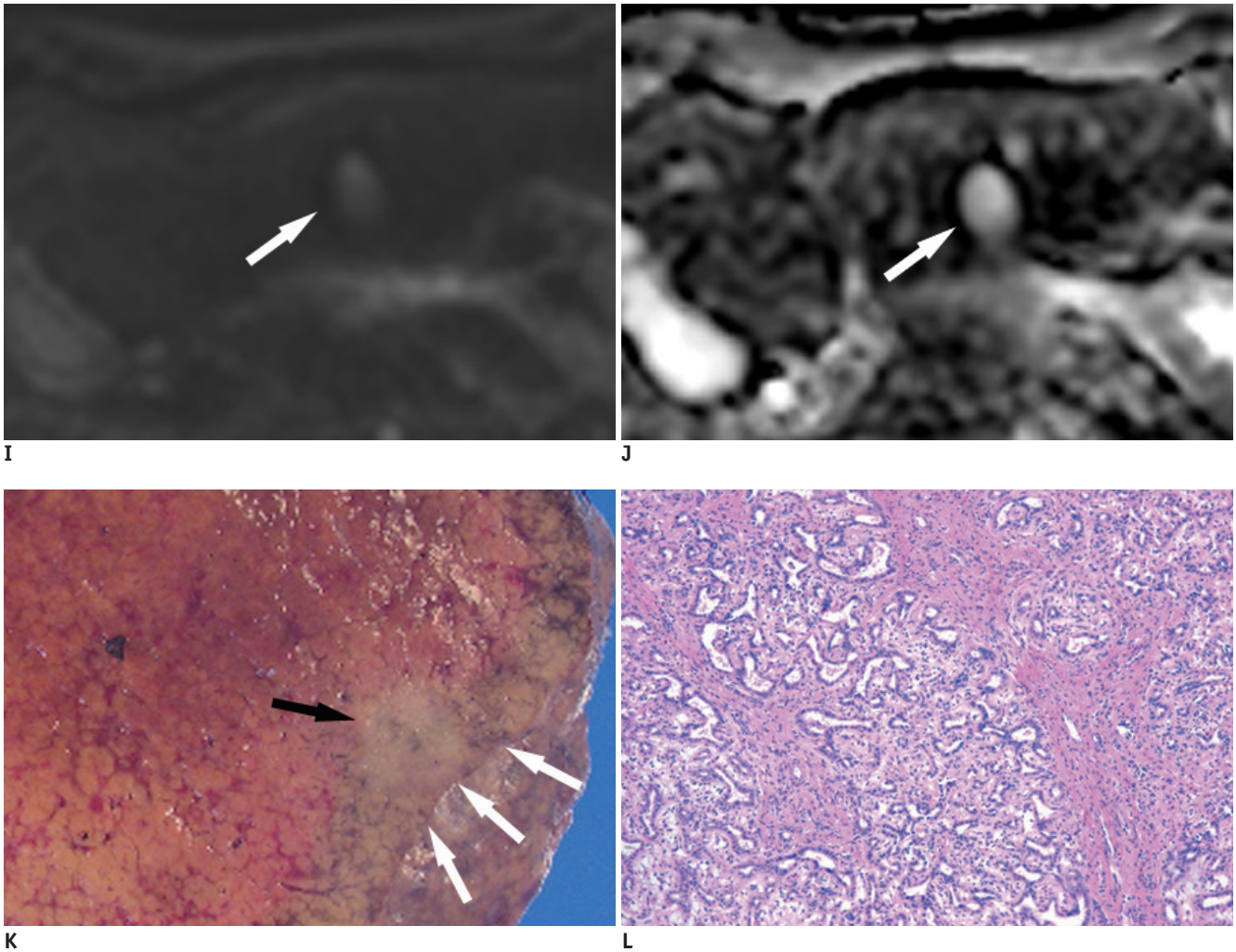

Fig. 1. Dynamic contrast-enhanced CT images, Gd-EOB-DTPA-enhanced and diffusion-weighted MR images, and pathologic findings in 64-year-old male with intrahepatic bile duct adenoma.
Gross and microscopic appearances of the tumor. **I, J.** On high b-value (800 s/mm^2) DWI **(I)** and on ADC map **(J)**, lesion (arrow) shows hyperintensity compared to liver parenchyma, indicating that diffusivity within lesion is increased and hyperintensity on DWI is due to T2 shine-through effects. **K.** Gross specimen shows ill-defined, non-encapsulated, yellowish-white nodule (black arrow) located immediately beneath hepatic capsule (white arrows). Surrounding liver parenchyma is congested and diffusely nodular. **L.** Microscopically, lesion consists of proliferation of well-formed bile ductules over background of fibrous stroma with several inflammatory cells coursing between ductules. No cellular atypia or mitotic activity is noted (Hematoxylin & Eosin staining, x 200). Gd-EOB-DTPA = gadolinium-ethoxybenzyl-diethylene triamine pentaacetic acid, DWI = diffusion-weighted imaging, ADC = apparent diffusion coefficient

Korean Journal of Radiology
KJR

DISCUSSION

Bile duct adenoma typically manifests as a small hypervascular tumor in patients with chronic liver disease undergoing HCC surveillance, which makes this rare benign tumor a HCC-mimicker on imaging studies (6). Thus, radiologists should be familiar with the radiologic features of BDA in order to avoid unnecessary surgery or other harmful treatments. Thus far, to our knowledge, eight cases of BDA that were diagnosed through imaging findings have been reported (7-10). In Table 1, we summarized the radiologic features of the eight previously reported cases as well as our case from the present study. All but one lesion (9 cm in size) were smaller than 2.1 cm (mean, 1.3 cm after excluding the 9 cm lesion), and all of the lesions were located in the subcapsular portion or on the surface of the liver. On MRI, the tumors showed variable signal intensities on T1-weighted images, on all but one lesion, which had calcification and showed hyperintensity on the T2-weighted images. On dynamic contrast-enhanced CT scans and conventional Gd-enhanced MRI, most BDAs were hypervascular with contrast-enhancement in the arterial and delayed phases. Delayed or persistent enhancement in dynamic imaging may be due to the fibrous stroma within the tumor (11). All three BDAs examined using Gd-EOB-DTPA-enhanced MRI showed relative hypo- or isointensity in the late dynamic phase and distinct hypointensity in the hepatobiliary phase, which may be explained by the lack

Table 1. Summary of Bile Duct Adenoma Cases from Literature and from Present Study

Case No./ Sex/Age	Reference	Location	Size (cm)	Ultrasound	Dynamic CT (Unenhanced/ Arterial/Delayed)	Conventional MRI (T1WI/T2WI)	Dynamic MRI (Arterial/ Delayed or Late Dynamic)	HBP of Gd-EOB-Enhanced MRI
1/F/62	Kobayashi et al., 1993*	Subcapsular region of right lobe	1.5	Hyperechoic with hypoechoic rim	Hyper/ NA/ hyper	NA	NA	NA
2/M/64	Miyazaki et al., 1997*	Surface of right lobe	1.7	Hyperechoic with hypoechoic rim	Hypo/ NA/ hypo with hyperdense rim	NA	NA	NA
3/M/75	Tajima et al., 1999 (7)	Surface of right lobe	0.5	Hyperechoic	NA/ hypo/ hypo	Mixed/ hyper	NA	NA
4/F/66	Tajima et al., 1999 (7)	Subcapsular regions of left lateral segment	1.4	Not visualized	NA/hypo/iso	Hyper/ hyper	Hyper/ hyper	NA
5/M/59	Tajima et al., 1999 (7)	Subcapsular regions of right lobe	0.4	Not visualized	NA/ hyper/ hyper	Hypo/ hyper	Hyper/ hyper	NA
6/F/78	Maeda et al., 2006 (10)	Subcapsular regions of right lobe	2	NA	Hyper (calcification)/ hyper/ hyper	Hypo/ hypo	NA	NA
7/F/59	Kim et al., 2010 (8)	Subcapsular regions of right lobe	1.7	NA	Hypo/ hyper/ hyper	Hypo/ hyper	Hyper/ hypo	Hypo
8/M/70	Koga et al., 2012 (9)	Left lobe	9	NA	Hypo/ hyper/ hyper	Hypo/ hyper	Hyper/ hypo	Hypo
9/M/64	Present study	Subcapsular regions of left lateral segment	1.4	NA	Hypo/ hyper/ iso	Hypo/ hyper	Hyper/ iso	Hypo

Note.— *Literature in Japanese. T1WI = T1-weighted image, T2WI = T2-weighted image, HBP = hepatobiliary phase, NA = non-assessable

of hepatocytes within the tumors. Thus, the enhancement pattern may not be sufficient to differentiate between BDA and HCC because some HCCs do not show venous washout, especially when they are small (< 2 cm) (12).

Our case is the first to be studied with DWI and shows that DWI may be useful for this differentiation. In our case, BDA showed hyperintensity on both high b-value DWI and the ADC map with an ADC value (2.21 x 10^{-3} mm^2/s) greater than the surrounding liver parenchyma (1.01 x 10^{-3} mm^2/s). This means that the observed hyperintensity on high b-value DWI was not due to restricted diffusion, but rather to T2 shine-through effects. Moreover, the overall diffusivity of the tumor was more than twofold that of the adjacent liver parenchyma (13). Several previous studies on the usefulness of DWI for differentiating between benign and malignant hepatic lesions demonstrated that malignant lesions, such as HCC and metastasis, may tend to have ADC values that are lower (e.g., typically < 2 x 10^{-3} mm^2/s) than benign lesions and non-tumorous liver parenchyma (14-19). A previous study also demonstrated that the histopathologic differentiation of HCC shows inverse correlation with the ADC value (20).

The high ADC value in our case may be explained by the microstructure of this particular tumor. Microscopically, BDA is characterized by a proliferation of tubulocystic structures (bile ductules) embedded in a fibrous stroma. In addition to the diffusion of water molecules in the ductules, the fibrous stroma may also have contributed to the high diffusivity of this lesion. Previous studies demonstrated that ADC of liver tissue gradually decreases as hepatic fibrosis progresses (21, 22). Recently, Mwangi et al. (23) measured and compared the ADC values of fibrous components and regenerative nodules through *ex vivo* and *in vivo* studies of cirrhotic livers. They demonstrated that the mean ADC value of fibrotic components was significantly greater than that of regenerative nodules or background cirrhotic liver parenchyma. The authors concluded that, contrary to prevailing notions, the reduced liver ADC value observed in cirrhosis is probably due to regenerative nodules rather than fibrotic bridges.

In summary, we experienced a case of BDA that was hypervascular and hepatocyte-defective on Gd-EOB-DTPA-enhanced MRI. On DWI, the tumor showed hyperintensity due to T2 shine-through effects on high b-value DWI and was also hyperintense on an ADC map with an ADC value greater than the surrounding cirrhotic liver parenchyma. Although we only report one case here, we believe that BDA may have inherently higher ADC values than the background liver because of its histologic features. We further suggest that DWI, along with ADC measurements, can be used as an important tool to reveal the benignity of BDA in clinical practice. Further diagnostic use of DWI with BDA cases is required to confirm our hypothesis.

REFERENCES

1. Bhathal PS, Hughes NR, Goodman ZD. The so-called bile duct adenoma is a peribiliary gland hamartoma. *Am J Surg Pathol* 1996;20:858-864
2. Edmondson HA. *Tumors of the liver and intrahepatic bile ducts*. In: Atlas of tumor pathology, fascicle 25. Washington DC: Armed Forces Institute of Pathology, 1958:19-29
3. Craig JR, Peters RL, Edmondson HA. *Tumors of the liver and intrahepatic bile ducts*. In: Atlas of tumor pathology, 2nd series. fascicle 26. Washington DC: Armed Forces Institute of Pathology, 1990:56-62
4. Allaire GS, Rabin L, Ishak KG, Sesterhenn IA. Bile duct adenoma. A study of 152 cases. *Am J Surg Pathol* 1988;12:708-715
5. Hornick JL, Lauwers GY, Odze RD. Immunohistochemistry can help distinguish metastatic pancreatic adenocarcinomas from bile duct adenomas and hamartomas of the liver. *Am J Surg Pathol* 2005;29:381-389
6. Lee JM, Zech CJ, Bolondi L, Jonas E, Kim MJ, Matsui O, et al. Consensus report of the 4th International Forum for Gadolinium-Ethoxybenzyl-Diethylenetriamine Pentaacetic Acid Magnetic Resonance Imaging. *Korean J Radiol* 2011;12:403-415
7. Tajima T, Honda H, Kuroiwa T, Yoshimitsu K, Irie H, Aibe H, et al. Radiologic features of intrahepatic bile duct adenoma: a look at the surface of the liver. *J Comput Assist Tomogr* 1999;23:690-695
8. Kim YS, Rha SE, Oh SN, Jung SE, Shin YR, Choi BG, et al. Imaging findings of intrahepatic bile duct adenoma (peribiliary gland hamartoma): a case report and literature review. *Korean J Radiol* 2010;11:560-565
9. Koga F, Tanaka H, Takamatsu S, Baba S, Takihara H, Hasegawa A, et al. A case of very large intrahepatic bile duct adenoma followed for 7 years. *World J Clin Oncol* 2012;3:63-66
10. Maeda E, Uozumi K, Kato N, Akahane M, Inoh S, Inoue Y, et al. Magnetic resonance findings of bile duct adenoma with calcification. *Radiat Med* 2006;24:459-462
11. Honda H, Onitsuka H, Yasumori K, Hayashi T, Ochiai K, Gibo M, et al. Intrahepatic peripheral cholangiocarcinoma: two-phased dynamic incremental CT and pathologic correlation. *J Comput Assist Tomogr* 1993;17:397-402
12. Forner A, Vilana R, Ayuso C, Bianchi L, Solé M, Ayuso JR, et al. Diagnosis of hepatic nodules 20 mm or smaller in cirrhosis: Prospective validation of the noninvasive diagnostic criteria for hepatocellular carcinoma. *Hepatology* 2008;47:97-104

13. Taouli B, Koh DM. Diffusion-weighted MR imaging of the liver. *Radiology* 2010;254:47-66
14. Feuerlein S, Pauls S, Juchems MS, Stuber T, Hoffmann MH, Brambs HJ, et al. Pitfalls in abdominal diffusion-weighted imaging: how predictive is restricted water diffusion for malignancy. *AJR Am J Roentgenol* 2009;193:1070-1076
15. Goshima S, Kanematsu M, Kondo H, Yokoyama R, Kajita K, Tsuge Y, et al. Diffusion-weighted imaging of the liver: optimizing b value for the detection and characterization of benign and malignant hepatic lesions. *J Magn Reson Imaging* 2008;28:691-697
16. Lee MH, Kim SH, Park MJ, Park CK, Rhim H. Gadoxetic acid-enhanced hepatobiliary phase MRI and high-b-value diffusion-weighted imaging to distinguish well-differentiated hepatocellular carcinomas from benign nodules in patients with chronic liver disease. *AJR Am J Roentgenol* 2011;197:W868-W875
17. Xu PJ, Yan FH, Wang JH, Shan Y, Ji Y, Chen CZ. Contribution of diffusion-weighted magnetic resonance imaging in the characterization of hepatocellular carcinomas and dysplastic nodules in cirrhotic liver. *J Comput Assist Tomogr* 2010;34:506-512
18. Muhi A, Ichikawa T, Motosugi U, Sano K, Matsuda M, Kitamura T, et al. High-b-value diffusion-weighted MR imaging of hepatocellular lesions: estimation of grade of malignancy of hepatocellular carcinoma. *J Magn Reson Imaging* 2009;30:1005-1011
19. Gourtsoyianni S, Papanikolaou N, Yarmenitis S, Maris T, Karantanas A, Gourtsoyiannis N. Respiratory gated diffusion-weighted imaging of the liver: value of apparent diffusion coefficient measurements in the differentiation between most commonly encountered benign and malignant focal liver lesions. *Eur Radiol* 2008;18:486-492
20. Heo SH, Jeong YY, Shin SS, Kim JW, Lim HS, Lee JH, et al. Apparent diffusion coefficient value of diffusion-weighted imaging for hepatocellular carcinoma: correlation with the histologic differentiation and the expression of vascular endothelial growth factor. *Korean J Radiol* 2010;11:295-303
21. Do RK, Chandarana H, Felker E, Hajdu CH, Babb JS, Kim D, et al. Diagnosis of liver fibrosis and cirrhosis with diffusion-weighted imaging: value of normalized apparent diffusion coefficient using the spleen as reference organ. *AJR Am J Roentgenol* 2010;195:671-676
22. Lewin M, Poujol-Robert A, Boëlle PY, Wendum D, Lasnier E, Viallon M, et al. Diffusion-weighted magnetic resonance imaging for the assessment of fibrosis in chronic hepatitis C. *Hepatology* 2007;46:658-665
23. Mwangi I, Hanna RF, Kased N, Malek P, Shiehmorteza M, Wolfson T, et al. Apparent diffusion coefficient of fibrosis and regenerative nodules in the cirrhotic liver at MRI. *AJR Am J Roentgenol* 2010;194:1515-1522